THE JOURNAL OF PHYSICAL CHEMISTRY A

Article

pubs.acs.org/JPCA

Sub-Doppler Spectroscopy of the *trans*-HOCO Radical in the OH Stretching Mode

Chih-Hsuan Chang, Grant T. Buckingham, and David J. Nesbitt*

JILA, National Institute of Standards and Technology, and Department of Chemistry and Biochemistry, University of Colorado at Boulder, Colorado 80309, United States

Supporting Information

ABSTRACT: Rovibrational spectroscopy of the fundamental OH stretching mode of the *trans*-HOCO radical has been studied via sub-Doppler high-resolution infrared laser absorption in a discharge slit-jet expansion. The *trans*-HOCO radical is formed by discharge dissociation of H_2O to form OH, which then combines with CO and cools in the Ne expansion to a rotational temperature of 13.0(6) K. Rigorous assignment of both a-type and b-type spectral transitions is made possible by two-line combination differences from microwave studies, with full rovibrational analysis of the spectrum based on a Watson asymmetric top Hamiltonian. Additionally, fine structure splittings of each line due to electron spin are completely resolved, thus permitting all three ε_{aa}, ε_{bb}, ε_{cc} spin−rotation constants to be experimentally determined in the vibrationally excited state. Furthermore, as both a- and b-type transitions for *trans*-HOCO are observed for the first time, the ratio of transition dipole moment projections along the *a* and *b* principal axes is determined to be μ_a/μ_b = 1.78(5), which is in close agreement with density functional quantum theoretical predictions (B3LYP/6-311++g(3df,3pd), μ_a/μ_b = 1.85). Finally, we note the energetic possibility in the *excited* OH stretch state for predissociation dynamics (i.e., *trans*-HOCO → H + CO_2), with the present sub-Doppler line widths providing a rigorous upper limit of >2.7 ns for the predissociation lifetime.

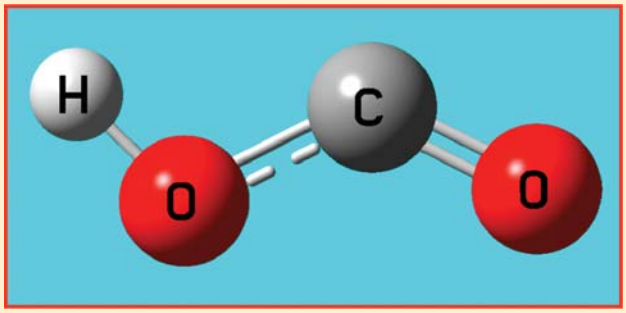

1. INTRODUCTION

The chemical reaction OH + CO → H + CO_2 (see Figure 1) has gained significant attention due its critical role in combustion chemistry[1] and indeed has been labeled the "second most important combustion reaction" in a review paper by Miller et al.[2] It is an overall strongly exothermic process and responsible for the final oxidative conversion step of CO to CO_2, a step which is clearly critical to achieving high efficiency levels of combustion. The unusual nature of this reaction is that it plays a critical and ubiquitous role in oxidative combustion of essentially all hydrocarbons, yet the reaction does not explicitly involve the actual hydrocarbon fuel at all. Despite its deceptive simplicity, this reaction is clearly far from elementary and is known to have multiple barriers, intermediates, and pathways along the reaction coordinate. This reaction and its many associated competing oxidative pathways also strongly impact levels of OH radical concentration in the atmosphere, mainly via oxidation of hydrocarbons to produce the peroxy radical, RO_2. Recent laboratory investigations by Li et al.[3,4] have revealed that current atmospheric models are not accurate enough to predict the correct concentration of OH radical in the atmospheric environment. Experimental evidence suggested that the chemical reaction of the electronic excited NO_2 with water may also provide the alternative pathway of generating the HO

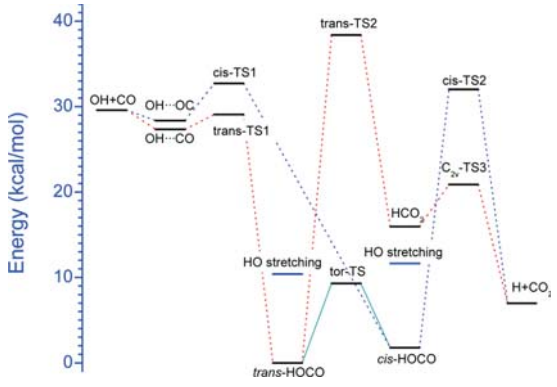

Figure 1. Local potential energy minima (kcal/mol) and transition state for trans and cis isomers of the HOCO radical. The energies of the ν_{OH} = 1 excited states for *trans*- and *cis*-HOCO are also shown, which indicate that both upper states are above the energetic limit for forming the asymptotic H + CO_2 product.

Special Issue: Terry A. Miller Festschrift

Received: April 5, 2013
Revised: May 23, 2013
Published: May 23, 2013

radical, which in turn plays a crucial role on the effect in the production of troposphere ozone.

The OH + CO reaction has a complex and distinguished history. Kinetic studies by Smith and Zellner[5,6] first revealed the non-Arrhenius behavior of this reaction, which displays a rate constant that increases with decreasing temperature between 210 and 460 K. A long-lived collision complex model was proposed to explain these experimental results, whereby slower collisions at a lower temperature would more efficiently access the region of phase space associated with the complex. The implicit assumption of a collision complex model was based on spectroscopic identification of *trans*-HOCO in the condensed phase, which was identified via matrix isolation by Jacox and co-workers.[7] On the basis of transition-state theory, Smith and Zellner were able to propose slight structural adjustments in the transition state and thereby successfully modeled the empirically observed rate constant behavior simply from a thermal perspective.

Chemical reaction dynamics of OH + CO → H + CO_2 and its reverse process have also been studied by Alagia et al.[8] and Brouad et al.[9,10] under molecular beam conditions. Their results indicate that this reaction is complex and exhibits nonstatistical behavior. Alagia et al. were able to estimate that roughly 65% of the available energy to form H + CO_2 must be partitioned into the translational degree of freedom. However, the structure of this intermediate complex had not been clearly identified. As shown in Figure 1, there are several possible candidates for the complex intermediate, which has been dubbed the HOCO radical. Hence, the desire to structurally identify these [HOCO]* intermediates had trigged considerable experimental and theoretical spectroscopic research. The low-energy barrier HO−CO orientation of the complex is apparently responsible for the formation of the trans complex in early stages, as confirmed by measurements by Lester and co-workers[11] using infrared action spectroscopy, which reveals the existence of the linear complex structure with a binding energy estimated to be 430 cm^{-1}. For the more covalently bound HOCO radical, however, the structure can be either trans or cis, as shown in Figure 2.

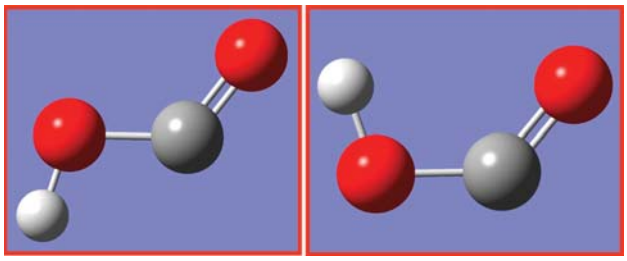

Figure 2. Schematic structures for (a) trans and (b) cis forms of the HOCO radical. Only IR spectra for the OH stretching mode of the *trans*-HOCO conformer are reported in the current high-resolution studies. To date, there has been no gas-phase spectral detection of the corresponding OH stretching mode for the *cis*-HOCO conformer.

The study of pure rotational spectra and laser magnetic resonance spectra of the *trans*-HOCO and DOCO enabled Sears and co-workers[12−14] to determined centrifugal distortion, spin−rotation constants, as well as a hyperfine constant with the laser magnetic resonance (LMR). Petty and Moore[15,16] determined the fundamental frequencies of O−H stretching of *trans*-HOCO and DOCH by time-resolved infrared spectroscopy (IR). Recently, Oyama et al.[17] determined the hyperfine structure of both trans and cis forms of HOCO radicals by Fourier transform (FT) microwave spectroscopy and millimeter-wave double-resonance techniques. Furthermore, they also observed the microwave spectra of the CO−*trans*-HOCO complex. The experimental observation reveals that the additional CO has almost no effect on the proton spin density for HOCO.[18] The fundamental frequencies of the trans and cis forms of HOCO had been identified by Jacox and co-workers in Ar, Ne, and CO matrixes.[7,19,20] Interestingly, however, reports for corresponding infrared detection of the *cis*-HOCO conformer in the gas phase have been conspicuously absent.

Using completely different approaches, Continetti and co-workers[21] have determined the fundamental frequencies of HOC bending, OC stretching, and OCO bending of *trans*-HOCO and isotopically substituted species with cryogenic ion trap photoelectron−photofragment coincidence spectroscopy. In addition to probing vibrational frequencies of the trans form, the bending modes of the *cis*-HOCO have also been possible to determine. The reason for this is that the cis form of the $HOCO^-$ anion is also populated in their source, from which photodetachment excitation of the electronic wave function projects significantly onto the neutral *cis*-HOCO frame via the Franck−Condon principle. From the experimentally measured electron affinities for both forms, the binding well depths with respect to the OH + CO fragmentation asymptote have been obtained, which are 1.07(2) eV for *trans*-HOCO and 0.99(2) eV for *cis*-HOCO. Fortenberry et al.[22−24] recently also published a series of state-of-the-art theoretical predictions for vibrational frequencies using high accuracy quantum chemical coupled cluster techniques and quartic force field calculations, which yield a remarkably small residual standard deviation (∼5 cm^{-1}) between theory and experiment. Such calculations demonstrate the current computational feasibility of obtaining a high-accuracy potential energy surface with high-level ab initio methods and basis sets.[25] The experimental and theoretical values for the fundamental frequencies of both *trans*-HOCO and *cis*-HOCO are summarized in Table 1.

In addition to spectroscopic efforts devoted to characterizing trans and cis forms of the HOCO radical, the actual chemical conversion from OH + CO reactants to H + CO_2 products has also been the focus of much attention. Specifically, Continetti and co-workers[26,27] studied dissociative photodetachment spectroscopy of the $HOCO^-$ anion and concluded that quantum tunneling effects promoted by OH stretch excitation at energies well below the calculated transition-state barrier may be an very important process in accessing the H + CO_2 exit channel. This experimental observation was later supported by theoretical calculations[28] by Guo and co-workers based on an accurate, entirely ab initio potential energy surface.[29] By way of further confirmation of the relevance of such tunneling dynamics in the exit channel, ab initio thermal rate constants calculated by Nguyen et al.[30] also agree quite well with the available experimental data, which cover a range in temperature that includes both combustion and terrestrial atmospheric chemistry. Specifically, the calculations indicate that H + CO_2 exit channel tunneling effects are indeed likely to be very important below 1000 K and indeed increase markedly in importance at the much lower temperatures relevant to atmospheric chemistry. What makes this dynamically interesting is that the H + OCO exit channel barrier is much closer to the *cis*-HOCO rather than *trans*-HOCO conformer (see Figure 1). As a result, tunneling lifetimes of the *cis*- versus *trans*-

Table 1. Summary of Theoretical Predictions and Experimental Observations of the Fundamental Vibrational Frequencies for trans and cis Conformers of the HOCO Radical

		trans-HOCO			*cis*-HOCO		
modes	description	Fortenberry et al.[a]	CO matrix[b]	gas	Fortenberry et al.[c]	CO matrix[b]	gas
ν_1	a′ O−H stretch	3636.0	3456	3635.702[d]	3446.1	3316	
ν_2	a′ C═O stretch	1855.8	1833	1852.567[e]	1816.6	1797	
ν_3	a′ H−O−C bend	1512.9	1261	1210.4	1282.7	1261	1290[f]
ν_4	a′ C−O stretch	1048.2	1077	1050	1040.3	1088	1040[f]
ν_5	a′ O−C−O bend	614.5	615	614	598.8	620	605[f]
ν_6	a″ torsional	501.8		508	564.2		

[a]Reference 36. [b]Reference 7. [c]Reference 23. [d]Reference 15. [e]Reference 13. [f]Reference 21.

HOCO forms might be anticipated to depend strongly on vibrational quantum state excitation, which could be seen in high-resolution IR spectroscopy of the corresponding isomeric species. Conversely, rapid predissociation dynamics from either the cis or trans isomer in excited vibrational states could also dramatically limit our experimental ability to probe HOCO via sub-Doppler infrared spectroscopy in the slit-jet discharge expansion environment.

As a necessary first step, therefore, we demonstrate efficient formation, high-resolution detection, and improved spectral analysis of the *trans*-HOCO conformer. Specifically, this work reports on the fundamental OH stretching vibrational mode of *trans*-HOCO, investigated herein with supersonic cooling (13 K) and sub-Doppler resolution (60 MHz) in a tunable difference frequency discharge infrared spectrometer. With the combination of slit-jet absorption sensitivity and rotational cooling, we are able to observe the predominantly strong a-type transitions of the OH stretch band, as well as the much weaker b-type transitions undetected in previous studies by Petty and Moore.[15] In addition, the combination of sub-Doppler resolution and low rotational temperature in the slit-jet expansion enables us to completely resolve the electron spin−rotation structure in this radical and therefore determine the three diagonal spin−rotation constants (ε_{aa}, ε_{bb}, ε_{cc}) unambiguously in the upper vibrational state. From Boltzmann plots for integrated areas of the two band types, the ratio of vibrational transition dipole moments along the *a* and *b* principal axes can also be determined and compared with quantum theoretical predictions. These studies lay the essential groundwork for establishing necessary confidence in the *trans*-HOCO discharge chemistry, which will be the basis for an ongoing search in the OH stretching region for the elusive *cis*-HOCO radical.

2. EXPERIMENTAL SECTION

Details of the sub-Doppler resolution infrared spectrometer have been described elsewhere and need only be briefly summarized.[31,32] Tunable, narrow-band (<1 MHz) infrared radiation is generated via difference frequency generation (DFG) within the temperature-controlled PPLN crystal (50 mm × 10 mm, periodically poled $LiNbO_3$ crystal) via the combination of two continuous waves from a single-mode ring dye laser (<2 MHz line width, Spectra-Physics 380A with R6G dye) and an etalon-stabilized Ar^+ ion laser (Spectra-Physics Series 2000). The frequency range between 2500 and 4500 cm^{-1} is accessed by Ar^+ laser operation at 488 or 514 nm, scanning the oven temperature and poling period to achieve quasi-phase-matching conditions. Roughly half of the total IR power (~11 μW) is sent into the detection region 5 mm downstream of the slit-jet discharge jaw orifice (4 cm × 300 μm), multipassed 16 times with a Herriott cell for a 64 cm optical path length, and focused on a N_2-cooled InSb signal detector. The remaining half is monitored on a matched N_2-cooled InSb reference detector, with a home-built servo loop (1 MHz bandwidth) to subtract laser noise contributions common to both the signal and reference beams.

The *trans*-HOCO radical is generated by flowing a CO/Ne gas mixture saturated in a liquid water reservoir into the supersonic free jet stagnation region, with 50 kHz square wave modulation of the 500 V discharge voltage on the defining slit jaw orifice. The radical absorption signal is demodulated with phase-sensitive lock-in detection to suppress non-shot noise contributions at low frequencies, with the phase optimized by adjusting CO and H_2O partial pressures for a typical *trans*-HOCO line. The absorbance noise level is estimated to be 0.0011% rms in a 10 kHz detection bandwidth, which translates into a signal-to-noise ratio (S/N) ≈ 60 for strongest transitions and near shot noise limited absorbance sensitivities of $1.4 \times 10^{-7}/\sqrt{\text{Hz}}$. The reported frequencies are obtained by interpolating fringes from an ultrastable optical transfer marker cavity with a 250 MHz free spectral range (FSR), yielding a rms frequency reproducibility for a typical line of ~6 MHz. Absolute frequencies are calibrated with respect to the ν_3, $1_{01} \leftarrow 1_{10}$ absorption line for $H_2{}^{16}O$ at 3638.08223 cm^{-1}, also obtained in the same sub-Doppler slit-jet geometry.[33]

3. RESULTS AND ANALYSIS

Figure 3 presents a global overview spectrum of the jet-cooled *trans*-HOCO radical in the 3626−3644 cm^{-1} region corresponding to excitation of the OH mode, with small spectral gaps due to absorption of the difference frequency IR light by atmospheric water lines. Even at this global scale of resolution, a number of rotational progressions can be recognized and readily assigned to the *trans*-HOCO radical, with transitions in the $K_a = 0 \leftarrow 0$ sub-band labeled with conventional railroad diagrams. Note that at these slit-jet temperatures, the spectrum is dominated by a 13 K thermal population in the lower $K_a = 0$ manifold, with rotational progressions similarly dropping off rapidly above $N \approx 10$. Thus, the present work nicely complements previous studies of the fundamental OH stretching mode by Petty and Moore,[15] based on 193 nm photolysis of vinyl formic acid ($C_2H_3CO_2H$) and time-resolved flash kinetic infrared absorption spectroscopy. Specifically, the room-temperature *trans*-HOCO spectra in these earlier studies reflect transitions from significantly higher angular momentum states ($N \approx 25-55$, $K_a \leq 8$) than those populated in the jet-cooled spectra reported herein. Furthermore, the present combination of reduced spectral congestion and higher

dx.doi.org/10.1021/jp403386d | J. Phys. Chem. A 2013, 117, 13255−13264

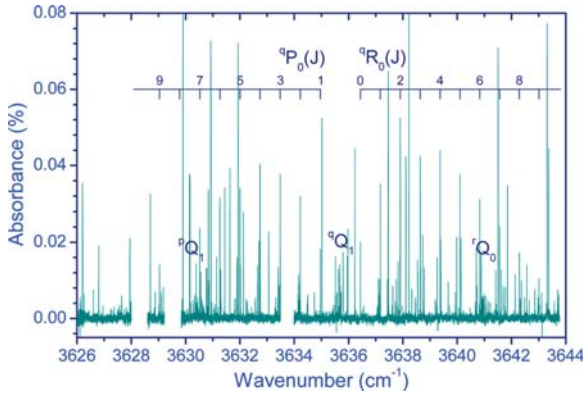

Figure 3. Jet-cooled and sub-Doppler rovibrational spectral transitions observed in the fundamental OH stretching region (~3635 cm^{-1}) for the *trans*-HOCO radical. Rotational quantum numbers for the dominant $^qP_0(N)$ and $^qR_0(N)$ branches are labeled, as well as approximate locations for the strongest $^pQ_1(N)$, $^qQ_1(N)$, and $^rQ_0(N)$ branches. Breaks in the spectral data are due to strong absorption lines of atmospheric water.

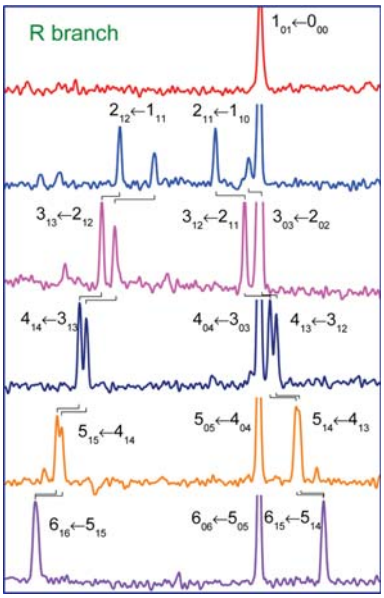

Figure 4. Systematic overlay of the high-resolution R branch scans for a-type transitions out of the K_a = 0 and 1 levels, clearly displaying sub-Doppler fine structure due to spin−rotation interactions. Transitions are arbitrarily registered with respect to the corresponding $^qR_0$ line for each value of the end-over-end angular momentum. The lines indicate the trend in spin−rotation splittings as a function of rotational energy, which for the present *trans*-HOCO a-type band, rapidly merges into a single unresolved line of approximately twice the intensity.

absorbance sensitivity permits the entire the OH stretch hybrid band (i.e., both a-type and b-type components) to be observed, assigned, and analyzed for the first time. Furthermore, the sub-Doppler spectral resolution in the slit-jet spectrometer permits the spin−rotation structure in each of the rotational transitions to be readily measured, which permits a detailed analysis of the fine structure splittings and spin−rotation tensor information for the vibrationally excited state. Finally, the use of sub-Doppler absorption methods permits a rigorous estimate of the upper limit for predissociation lifetime dynamics for *trans*-HOCO → H + CO_2 in the OH stretch vibrationally excited state.

In the present work, *trans*-HOCO is formed by collisions of the OH radical with CO in the slit-jet discharge expansion, with Ne atoms stabilizing the nascent hot HOCO radical by three-body relaxation. Peak absorbances for the *trans*-HOCO radical are estimated to be about ~0.06% for the strongest rovibrational lines, with a rotational temperature estimated to be 13.0(6) K from the analysis of the Boltzmann plot. By way of example, Figure 4 displays a systematic overlay of high-resolution scan regions for the K_a = 1 ← 1 and K_a = 0 ← 0 R branch sub-bands, where the additional spectral structure due to K_a = 1 asymmetry doubling and spin−rotation coupling is immediately evident. The asymmetry splitting in the K_a = 1 manifold increases as ~$[N(N+1)]^{1/2}$, which for an a-type band (ΔK_a = 0), as expected, results in asymmetry doubling that *increases* roughly linearly with the end-over-end rotational quantum number N. However, the corresponding spin−rotation structure in these asymmetry split transitions *decreases* rapidly with increasing quantum number N, as will be analyzed and discussed in more detail later. As a result, spin−rotation information in the *trans*-HOCO spectra is most accessible from the lowest rotational levels, which again are most favorably populated under supersonic jet-cooled conditions.

Figure 5a and b feature a similar high-resolution display of the Q branch region, which, due to supersonic jet cooling, is dominated by the lowest optically allowed transitions out of the K_a = 1 stack. Most importantly, the spectra clearly reveal both a-type and b-type transitions with S/N ≥ 10. Using near-symmetric top notation, we clearly observe two dominant b-type $^rQ_0(N)$ (Figure 5b) and $^pQ_1(N)$ (not shown here) sub-branches in the region near the band origin, with progressions of lines in the $^rP_0(N)$ and $^rR_0(N)$, $^pR_1(N)$ sub-branches identified and assigned despite the ~2-fold weaker P/R versus Q branch signal intensities. This is at first a bit surprising because only a-type band transitions were reported in Petty and Moore's early study, despite unambiguous predictions from their spectral fits for where the corresponding b-type band transitions should occur.[15] Indeed, given that the ratio of a-type/b-type band intensities is determined to be only ~3:1 in the current slit-jet spectra, it is not immediately clear why these b-type transitions were not observed previously. However, we can offer two possible suggestions. First of all, the *trans*-HOCO populations at room temperature are diluted into appreciably higher N and K_a levels, which, in conjunction with lower spectral congestion due to sub-Doppler resolution, may help explain the greater visibility for b-type transitions under slit-jet-cooled conditions. Second and more quantitatively, the a-type spin−rotation splittings for *trans*-HOCO blend with increasing rotational quantum number N into a single unresolved line and therefore generate a fortuitous 2-fold increase in peak intensity. By way of contrast, the b-type spin−rotation splittings remain fully resolved up to high N values, therefore eliminating such a 2-fold enhancement in signal strength for spectra obtained under room-temperature, Doppler-limited conditions.

From Figure 5a and b, additional spectral structure due to the spin−rotation interaction is also evident. As illustrated in the accompanying figure legend, there are four allowed spin−rotation transitions associated with a given N rotational quantum number for a Q branch. Indeed, for the very lowest optically allowed transitions out of N = 1 levels, one can indeed see evidence in Figure 5a for four a-type lines at sub-Doppler resolution. However, for N > 1 values, the spin−rotation transition intensities asymptotically approach the usual ΔN =

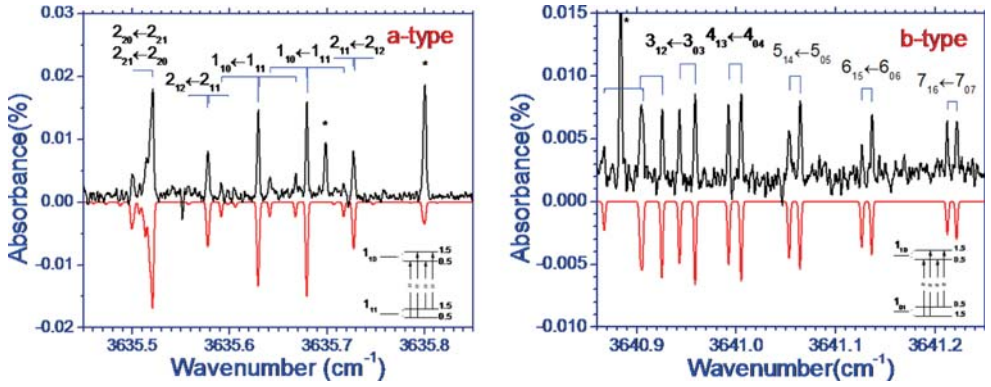

Figure 5. (a) The a-type Q branch progressions out of the K_a = 1 and 2 manifolds in the band origin region near 3635.7 cm^{-1}. Note that of the four allowed spin−rotation transitions, the two fine structure lines following the $\Delta N = \Delta J$ propensity rule are strongest and merge into an unresolved and 2-fold more intense peak with increasing N value. (b) A single b-type $^rQ_0(N)$ branch progression out of the K_a = 0 manifold. Note that the *trans*-HOCO spin−rotation interactions yield fully resolved fine structure splittings up to high N values. This reduces the signal intensity with respect to the a-type band by an additional factor of 2, which, in conjunction with spectral congestion, is likely responsible for lack of observation of any b-type band transitions in the previous studies of Petty and Moore.[15].

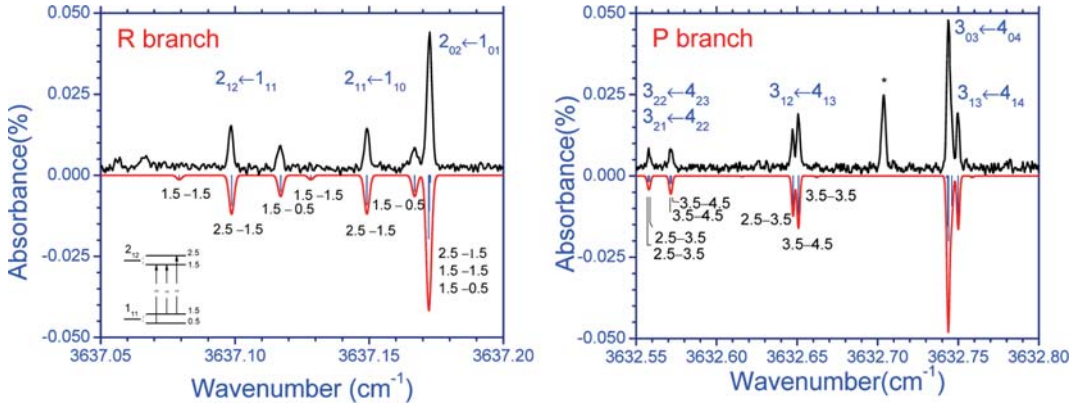

Figure 6. The a-type spin−rotation structure in the (a) N = 1, K_a = 0, 1 and (b) N = 4, K_a = 0, 1, 2 transition multiplets. The transitions are labeled by asymmetric top N_{KaKc} quantum numbers at the top, with the corresponding $J' \leftarrow J''$ components labeled below, with the stick plot and spectral simulation shown in blue and red, respectively. Note again that a-type spin−rotation splittings are systematically small and would therefore merge into single, unresolved lines with approximately twice the intensity under non-sub-Doppler conditions.

ΔJ = 0 propensity rule, where **J** = **N** + **S** in the Hund's case b$_J$ coupling scheme. In this limit, Q branch transitions for a-type and b-type bands are dominated by a pair of two strong ΔJ = 0 lines, whose splittings provide high-resolution information on the corresponding components of the spin−rotation tensor. Additional detailed spin−rotation information is obtained from the corresponding P and R branches, as illustrated in sample high-resolution scan regions shown in Figure 6a and b. In each of these branches, there are now only three optically allowed spin−rotation transitions but with the usual propensity rule $\Delta N = \Delta J = \pm 1$ resulting in only two dominant transitions out of all but the very lowest N levels.

Assignment of all spectral structures to both rotational ($N'_{Ka'Kc'} \leftarrow N''_{Ka'',Kc''}$) and spin−rotational quantum numbers (where $J = N \pm 1/2$) is straightforward, loosely guided by the rovibrational analysis of Petty and Moore and then rigorously confirmed by two-line combination differences from the precision microwave studies of Oyama et al.[17] A list of all assigned transitions is available in the Supporting Information. A-reduced Watson effective rotational Hamiltonian, including the effective spin−rotation interaction,[34] is used to analyze the rovibrational transitions. The effective Hamiltonian is

$$\begin{aligned} H_r = {} & AN_a^2 + BN_b^2 + CN_c^2 - \Delta_N N^4 - \Delta_{NK} N^2 N_a^2 - \Delta_K N_a^4 \\ & - (\delta_N N^2 + \delta_K N_a^2)(N_b^2 - N_c^2) \\ & - (N_b^2 - N_c^2)(\delta_N N^2 + \delta_K N_a^2) \\ & + \varepsilon_{aa} N_a S_a + \varepsilon_{bb} N_b S_b + \varepsilon_{cc} N_c S_c \end{aligned} \quad (1)$$

In eq 1, the top line reflects terms due to the rigid asymmetric top rotational energy (A, B, C), with the second line comprising the lowest fourth-order centrifugal distortion correction terms (Δ_N, Δ_{NK}, Δ_K, δ_N, δ_K). The third line contains diagonal spin−rotation interaction contributions (ε_{aa}, ε_{bb}, ε_{cc}), which are the only nonvanishing terms for a molecule with orthorhombic symmetry. Additional hyperfine interactions due to nuclear spin (e.g., isotropic Fermi contact terms due to the H atom) are predicted to be on the order of 10−20 MHz and thus too small to be significant even with 60 MHz sub-Doppler resolution.

The ground-state asymmetric top and spin−rotation constants are fixed at values from the Oyama et al. microwave study,[17] while constants for the upper state are floated in a nonlinear least-squares fitting to all a-type, b-type, and spin−rotation resolved transitions. The final results for these molecular constants as well as the vibrational band origin

Table 2. Molecular Constants for *trans*-HOCO in the Ground State and First Excited OH Stretching Level

	ground state			ν_{OH} = 1 stretching state	
vibration	calculation[a]	LMR[b]	microwave[c]	flash kinetic spectroscopy[d]	sub-Doppler, slit-jet supersonic discharge
A	5.61276	5.5960782(64)	5.596140(1)	5.54790(13)	5.55158(7)
B	0.38188	0.3813800(21)	0.381375(1)	0.381026(11)	0.381015(2)
C	0.35698	0.3564640(21)	0.356468(1)	0.3559852(74)	0.355990(3)
Δ_N[e] $\times 10^7$		3.033(18)	2.96(1)	2.76(17)	2.35(19)
$\Delta_{NK} \times 10^6$		−9.882(11)	−9.884(7)	−9.24(28)	−3.33(115)
$\Delta_K \times 10^4$		7.8689(33)	7.86891(3)	7.337(21)	7.19(14)
$\delta_N \times 10^8$		4.10(11)	3.37(2)	3.8(1.4)	*e*
$\delta_K \times 10^6$		3.67(89)	3.6(3)	*f*	*e*
$\Phi_N \times 10^{11}$			−1.6(6)		
$\Phi_{KN} \times 10^9$		−4.69(16)	−4.7(1)	*f*	
ε_{aa}		0.051661(53)	0.0517165(9)	0.0516(11)	0.05121(7)
ε_{bb}		0.000319(17)	0.000319[b]	*f*	0.00030(2)
ε_{cc}		−0.000914(27)	−0.0009075(1)	*f*	−0.00081(2)
a_F			−0.0002295(1)		
T_{aa}			0.0000778(3)		
T_{bb}			−0.000176(3)		
T_{ab}			0.000390(3)		
$\Delta^S_k \times 10^5$		−1.802(70)	−1.86(2)		
Δ		+0.076[g]	+0.076[g]		+0.073[g]
ν_0				3635.7020(15)	3635.69930(5)

[a]Reference 36. [b]Reference 12. [c]Reference 17. [d]Reference 15. [e]Fixed at microwave values. [f]Fixed at values from LMR studies. [g]Inertial defect $\Delta \equiv I_{cc} - I_{bb} - I_{aa}$ (unit in amu·Å^2).

(ν_0) are summarized in Table 2, with results from previous LMR, FT microwave, and IR studies also included.[12,15,35] Under the present jet-cooled conditions with relatively small N and K_a values, the weaker asymmetric top quadratic distortion constants δ_N and δ_K for the upper state are not reliably determined and are thus held fixed at the ground-state microwave values. Though there are small differences between the current sub-Doppler analysis and previous reports for the upper state, the agreement is generally excellent. Indeed, the fortuitous combination of low congestion due to supersonic jet cooling, sub-Doppler spectral resolution, as well as inclusion of both a-type and b-type transitions in the least-squares fits makes for a significantly improved spectral analysis. In particular, this permits all three spin−rotation constants to be determined with high precision in the vibrationally excited state, as summarized in Table 2 and discussed in more detail below.

4. DISCUSSION

A. *trans*-HOCO Molecular Constants. In the present work, both a-type and b-type hybrid bands as well as spin−rotational splitting are observed and resolved experimentally, which enables a significantly improved determination of the low-order molecular constants. This is to be expected as the previous flash kinetic measurements[15] involve fitting to high N states populated at near or above room temperature, as opposed to the very much lower energy N states thermally available under supersonically cooled expansion conditions and with sub-Doppler resolution. The present least-squares fitting results are shown in Table 2. The band origin for the fundamental OH stretching mode of *trans*-HOCO is found to be 3635.69930(5) cm^{-1}, which is in excellent agreement with theoretical predictions of 3636.0 cm^{-1} by Fortenberry et al.,[36] 3639.6 cm^{-1} by Wang et al.,[37] as well as results of the previous experimental study by Petty and Moore[15] of 3635.7020(15) cm^{-1}. The most significant difference (i.e., >3 σ) between the two experimental sets of end-over-end rotational constants lies in the determination of A, which the present work specifies with much improved precision due to simultaneous observation of both a-type and b-type transitions. Furthermore, the sub-Doppler capability of the current slit-jet expansion geometry permits complete resolution and least-squares fitting of the spin−rotation constants, yielding precision experimental results for all three values in the vibrationally excited state, specifically ε_{aa} = 0.05121(7), ε_{bb} = 0.00030(2), and ε_{cc} = −0.00081(2) cm^{-1}. Because the spin−rotation interaction is thought to be dominated by second-order electronic interactions, this yields valuable information on the excited-state energy level structure, as will be addressed later in the Discussion section.

For a perfectly rigid, flat object, the inertial defect ($\Delta \equiv I_{cc} - I_{bb} - I_{aa}$) can be readily shown to vanish identically. However, this is not rigorously true for real molecules with only planar equilibrium geometries when one also includes the finite mass of the electron cloud and zero-point rovibrational displacements away from planarity. Indeed, Oka and Morino[38] showed that there are mainly three physical sources that contribute to the experimental observation of the finite inertial defect, specifically (i) vibrational, (ii) electronic, and (iii) centrifugal distortion terms. The centrifugal correction depends on higher-order rotationally induced distortion of the nuclei positions; this can be estimated to be quite small (<10^{-4} amu·Å^2) for most molecular systems[39] and therefore plays only a relatively minor role. Also small but more significant is the electron cloud, which systematically yields a negative contribution due to finite mass density away from the nuclear plane.[38] However, the largest corrections typically originate from a combination of finite in-plane versus out-of-plane quantum motion of the nuclei, either due to quanta of vibrational excitation or even just at the zero-point level. In the case of the *trans*-HOCO radical, the inertial defect for the ground-state zero-point vibrational

level is estimated to be +0.076 amu·Å^2 from LMR and microwave studies, which is indeed the correct sign anticipated for large-amplitude in-plane bending modes with heavy atoms. For ν = 1 OH vibrational excitation of *trans*-HOCO, this predominantly in-plane OH stretch results mainly in a change in moments of inertia along the *b*- and *c*-axis. The upper state inertial defect is determined to be 0.073 amu·Å^2, that is, reflecting a small *decrease* (−3.9%) due to excitation of large-amplitude in-plane motion.

Fine structure comes from the coupling of the unpaired electron spin (**S**) to the molecular end-over-end rotation angular momentum(**N**) of the radical system.[34,40] It has been shown[34,40,41] that there are two physical contributions to such fine structure interaction. This first contribution is relatively weak and based on direct first-order interaction between the electron spin magnetic moment with the magnetic field generated by tumbling rotation.[42] However, the much larger effect is thought to arise from second-order mixing of excited rovibronic states through electronic Coriolis interactions. The experimentally measured spin−rotational constants provide invaluable information about the symmetry and energetic position for the excited electronic state. For example, as shown in Table 2, the dominant term, ε_{aa}, is mainly influenced by the energy of the first excited^{2}A″ state. The first ^{2}A″ excited state for *trans*-HOCO was predicted by Sears et al.[12] to lie ∼36 kcal/mol above the ground state, based on the simple assumption of similar electronic state behavior for HCO and *trans*-HOCO radicals. Li and Francisco[43] subsequently performed these calculation using CCSD(T) methods and cc-pVDZ and cc-pVTZ basis sets, which predicted this excitation to be ∼71 kcal/mol, that is, considerably higher. This work also revealed that discrepancies between these two calculations could arise from significant differences in vertical excitation energies, specifically 2.2 eV (50.7 kcal/mol) and 4.2 eV (96.6 kcal/mol), predicted for HCO and *trans*-HOCO radicals, respectively. Interestingly, the Li and Francesco calculations also suggested this first excited ^{2}A″ state to exhibit significant predissociation dynamics correlating with the entrance channel OH($X^2\Pi$) + CO($^1\Sigma^+$) limit. Experimental support of this much higher energy prediction was later provided by dissociative photodetachment studies of Continetti and co-workers.[44,45]

B. OH Stretch a-Type/b-Type Band Intensity Ratio. This jet-cooled study represents first spectral detection of both a-type and b-type components in the OH stretch hybrid band, which makes it possible to estimate the ratio of vibrational transition dipole moments along the molecule frame *a*- and *b*-axes, respectively. In order to achieve such an estimate, we perform separate Boltzmann simulations for each of the a-type and b-type absorption line data. In particular, the integrated intensity for a given i ← j absorption line in a thermally equilibrated sample is well described by

$$S_{ij} = C_{ij} \cdot g_N \cdot \mathrm{HL} \cdot \exp(-E_{rot}/kT) \quad (2)$$

In eq 2, S_{ij} reflects a sum over all intensity contributions due to spin−rotation structure, C_{ij} is a coefficient proportional to the a-type or b-type vibrational dipole transition moment $|\mu_a|^2$or $|\mu_b|^2$, g_N is the 2N + 1 rotational degeneracy of the rotational level, HL the generalized Hönl−London factor for an $N'_{Ka'Kc'} \leftarrow N''_{Ka'',Kc''}$ asymmetric top transition, and $\exp(-E_{rot}/kT)$ is the usual Boltzmann factor at a temperature T for the lower state. Figure 7 displays the corresponding Boltzmann plots of $\ln[S_{ij}/g_N/\mathrm{HL}]$ versus E_{rot}, which have been least-squares fit for a- and b-band types to a common rotational temperature of T_{rot} = 13.0(6) K. The difference between the two *y*-intercepts, as shown in Figure 7 and experimentally determined from multiple scans, yields the logarithm of the a-type to b-type transition dipole moment ratio, which permits extraction of $|\mu_a/\mu_b|^2$ = 3.16(10) and thus $|\mu_a/\mu_b|$ = 1.78(5). Indeed, this $|\mu_a/\mu_b|$ value is in remarkably quantitative agreement with Gaussian 09 theoretical predictions (B3LYP/6-311++g(3df,3pd)) of $|\mu_a/\mu_b|$ = 1.85, obtained from the dot product of the dipole moment derivative vector for the OH stretching vibration with unit vectors along the *a* and *b* principal axes. Interestingly, the b-type band intensity for the OH stretch would appear to be down only by ∼3-fold from the a-type band, which makes it a bit surprising that it was not observed in the previous flash kinetic efforts.[15] However, on the basis of the spectral data in Figure 5b, these b-type band transitions are quite readily detectable under the much lower temperatures, sub-Doppler resolution, and lower spectral congestion obtained with the slit-jet discharge expansion source.

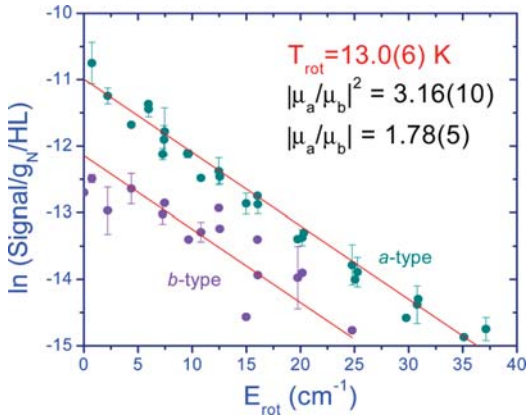

Figure 7. Boltzmann plot for the a-type and b-type band rovibrational transition intensities. The slope from a combined least-squares fit to the two bands is consistent with a common rotational temperature of 13.0(6) K, with the intercepts indicating the ratio of a-type to b-type integrated band intensities to be $|\mu_a/\mu_b|^2$ = 3.16(10).

C. Initial Search for *cis*-HOCO Spectra in the OH Stretch Mode. We briefly return to the issue of gas-phase spectral detection for both *trans*- and *cis*-HOCO conformers possible in our slit-jet discharge expansion. As indicated in the Figures 1 and 2, it is possible for the HOCO radical to exist in both trans and cis structures, with the *cis*-HOCO minimum theoretically predicted to be ΔE = 1.77 kcal/mol energetically above *trans*-HOCO. This is only a modest energy difference compared to kT under typical combustion temperature conditions, and thus, these two conformers can both be dynamically important. However, a sizable ∼9.3 kcal/mol barrier separating the trans from the cis configuration is also predicted, which would significantly slow rates of collisional interconversion and equilibration. Thus, it is not at all clear how rapidly populations between these two isomer wells can interconvert and/or reach an equilibrium status, either at the extremely low temperatures of a supersonic expansion or the much higher temperatures relevant to combustion.

It is well worth noting in this regard is that *both* ground vibrational state *trans*-HOCO and *cis*-HOCO isomers have been spectrally identified in the microwave rotational work by Oyama et al., under the same, low-temperature conditions of a supersonic pinhole expansion.[17] From relative intensities of the two rotational spectra, they estimated approximately equal

dx.doi.org/10.1021/jp403386d | J. Phys. Chem. A 2013, 117, 13255−13264

formation of the trans and cis isomers from OH + CO reactions in their pinhole discharges. Thus, clearly, both isomers are stable with respect to dissociation into the H + CO_2 product channel, at least for the vibrationless ground state. There is no experimental evidence, however, on the stability of *trans*- or *cis*-HOCO in the OH stretch vibrationally excited state, which would significantly impact feasibility for detection via high-resolution methods. Indeed, the dynamics of *cis*- and *trans*-HOCO in their ground and vibrationally excited states represents an ongoing challenge for both experiment and theory. Alternatively stated, the success of obtaining such spectra for *cis*-HOCO in condensed-phase matrixes yet a corresponding failure (to date) in the gas phase makes high-resolution infrared detection of *cis*-HOCO a topic of considerable interest.

By way of preliminary effort, we have performed a high-resolution IR search for the *cis*-HOCO isomer in the OH stretch region, guided by predictions from both high-level theory[23] as well as experimental matrix studies by Jacox and co-workers.[7,19,20] For measurements of the *trans*-HOCO rovibrational transitions discussed above, the typical signal-to-noise ratio for a strong peak is S/N ≈ 60:1. According to Huang et al.'s calculations,[46] the predicted integrated OH stretch band intensities for *trans*-HOCO and *cis*-HOCO should be 80.3 and 14.9 km/mol, respectively. Thus, if we take such a ∼5.4-fold difference in absorbance strength into account, this would imply that *cis*-HOCO isomer concentrations in our slit-jet must be at least 11 times smaller than those of *trans*-HOCO to remain undetected under the present sensitivity conditions. We are currently in the process of pursuing alternative precursors for increasing OH concentrations to provide an additional improvement in both *trans*- and *cis*-HOCO isomer signals.

We can, however, offer the following observations. If the isomer populations were equilibrated to the observed T_{rot} ≈ 13 K rotational temperature, the ∼1.77 kcal/mol energy difference would correspond to a $\sim 10^{-30}$ ratio of *cis*-HOCO to *trans*-HOCO, that is, far lower than any conceivable experimental sensitivity levels. By way of a counter example, both ground-state *trans*- and *cis*-HOCO species are detectable in pinhole discharge expansions, which implies that true thermal "equilibration" between forward and reverse barrier crossings is clearly not always maintained. However, the number of strong, thermalizing collisions in a supersonic jet can be dramatically different for pinhole versus slit expansion geometries. Specifically, the slit-jet versus pinhole environment offers a much slower ($1/r$ versus $1/r^2$) drop-off in expansion density, which for HOCO would typically translate into 1−2 orders of magnitude more cooling collisions prior to the freeze-in region.[47] In many van der Waals complexes, for example, this additional boost in slit-jet collision frequency proves sufficient to maintain essentially complete thermalization of rotation and vibration, at least up to relatively low frequencies of ∼667 cm^{-1}.[48−51] Whether this represents sufficient collision numbers to begin to equilibrate *cis*- and *trans*-HOCO isomer populations over a 9.3 kcal/mol barrier is not clear. It is worth noting that requisite reduction of *cis*-HOCO versus *trans*-HOCO populations consistent with our present sensitivity levels would only require "cooling" a presumed equilibrium isomer distribution to ∼370 K. One plausible dynamical scenario is that the increased number of collisions in the slit-jet expansion relaxes HOCO from the OH + CO direction into the trans potential well more efficiently, with the *trans*-HOCO then experiencing strong collisions too infrequently at these low jet temperatures to surmount the barrier to form the *cis*-HOCO isomer. Another potential path for accessing the *cis*-HOCO well could come from H + CO_2 reagents in the reverse direction, though this would requires overcoming an even larger barrier (ΔE_{rev} ≈ 25 kcal/mol) than for the OH + CO forward direction (ΔE_{for} ≈ 9 kcal/mol).

As a final comment, it bears noting from Figure 1 that the OH stretch excitation of both *trans*- and *cis*-HOCO is theoretically predicted to be above the limit to H + CO_2 formation, which could therefore lead to predissociation from metastable vibrationally excited states.[21,26,30,52] The current sub-Doppler linewidths (<60 MHz) observed in the slit-jet provide a rigorous lower limit to such a dissociation lifetime of >2.7 ns for the *trans*-HOCO isomer. What the corresponding lifetime might be for the *cis*-HOCO isomer is clearly not well understood, although one could reasonably argue that it would be shorter than that for *trans*-HOCO becaue (i) the OH stretch is largely parallel to the dissociation coordinate and (ii) the cis well is separated only by a single rather than a double barrier from H + OCO products (see Figure 1). It is additionally worth noting, of course, that any predissociation dynamics with lifetimes < 2.7 ns will yield additional line broadening beyond our sub-Doppler limit, with concomitant reduction in peak spectral absorbance and detection sensitivity for the *cis*-HOCO versus *trans*-HOCO isomer. Thus, one intriguing possibility would be that the high-resolution infrared spectrum of *cis*-HOCO is sufficiently broadened by tunneling dissociation dynamics to fall below our current S/N limit. In any event, we hope that the present work will stimulate further experimental and theoretical efforts in these directions, from which we can elucidate further details of the potential energy surface for both *trans*- and *cis*-HOCO, as well as possible reaction dynamics as a function of the isomer and vibrational quantum state.

5. SUMMARY AND CONCLUSION

The combination of high radical density and high detection sensitivity in the slit-jet discharge infrared spectrometer has been used to explore the fundamental OH stretching mode for the jet-cooled *trans*-HOCO radical under sub-Doppler resolution conditions. In these initial studies, the HOCO radical has been formed via discharge of H_2O to form OH, which, under slit-jet expansion conditions, in turn reacts with CO to make significant concentrations of the *trans*-HOCO form. Each rovibrational transition in *trans*-HOCO exhibits additional fine structure splittings due to open-shell spin−rotation interactions, which permits the three nonvanishing components of the spin−rotation tensor to be determined experimentally. Additionally, b-type as well as a-type transitions are identified in this study for the first time, which provides additional information and accuracy for analysis of both fundamental rovibrational constants and spin−rotation interactions. The low temperature of the slit-jet expansion has also been exploited to determine the ratio of a-type to b-type band intensities via detailed Boltzmann analysis of the rotational line strengths The ratio of vibrational transition dipole moment along the *a*- and *b*-axis is determined to be $|\mu_a/\mu_b| = 1.78(5)$, which is in excellent agreement with simple DFT calculations ($|\mu_a/\mu_b| = 1.85$) and provides valuable information with which to compare and evaluate more sophisticated level quantum theoretical treatments (see Figure 8). Indeed, it is our hope that these high-resolution IR studies of *trans*-HOCO and future studies of *cis*-HOCO will offer the necessary quantitative metrics for both validating and improving the state of the art ab

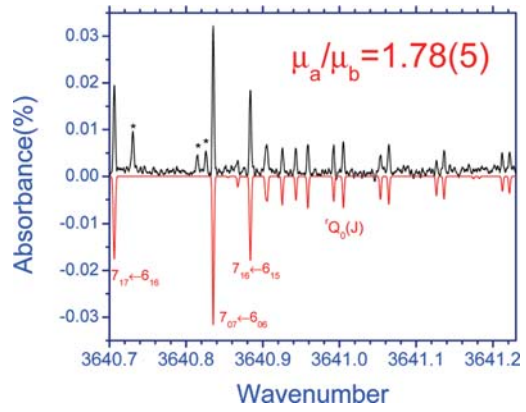

Figure 8. (a) Spectral simulation for accidentally overlapping a-type [$^rR_{0,1}(6)$] and b-type [$^rQ_0(N)$] transitions in the OH stretching fundamental band, with the ratio of transition dipole moments ($|\mu_a/\mu_b|$ = 1.78(5)) and rotational temperature (T_{rot} = 13.0(6)K) taken from the accompanying Boltzmann plot in Figure 7. Interloper transitions not assigned to *trans*-HOCO are marked with ∗.

initio predictions of Francisco, Lee, and co-workers, as well as testing the recent permutationally invariant potential energy and dipole moment surfaces of Bowman and co-workers.[24,36,37,46]

■ ASSOCIATED CONTENT

Supporting Information

A complete table of sub-Doppler transition frequencies and assignments for both a- and b-type OH stretch vibrational bands in *trans*-HOCO. This material is available free of charge via the Internet at http://pubs.acs.org.

■ AUTHOR INFORMATION

Notes

The authors declare no competing financial interest.

■ ACKNOWLEDGMENTS

This work was supported by grants from the Department of Energy (DE-FG02-09ER16021), with initial funds for construction of the slit-jet laser spectrometer provided by the National Science Foundation (CHE 1012685, PHY 1125844).

■ REFERENCES

(1) Francisco, J. S.; Muckerman, J. T.; Yu, H.-G. HOCO Radical Chemistry. *Acc. Chem. Res.* **2012**, *43*, 1519−1526.
(2) Miller, J. A.; Kee, R. J.; Westbrook, C. K. Chemical Kinetics and Combustion Modeling. *Annu. Rev. Phys. Chem.* **1990**, *41*, 345−387.
(3) Li, S.; Matthews, J.; Sinha, A. Atmospheric Hydroxyl Radical Production from Electronically Excited NO_2 and H_2O. *Science* **2008**, *319*, 1657−1660.
(4) Wennberg, P. O.; Dabdub, D. Rethinking Ozone Production. *Science* **2008**, *319*, 1624−1625.
(5) Smith, I. W. M.; Zellner, R. Rate Measurements of Reactions of OH by Resonance Absorption. Part 2.—Reactions of OH with CO, C_2H_4 and C_2H_2. *J. Chem. Soc., Faraday Trans.* **1973**, *69*, 1617−1627.
(6) Smith, I. W. M. The Mechanism of the OH + CO Reaction and the Stability of the HOCO Radical. *Chem. Phys. Lett.* **1977**, *49*, 112−115.
(7) Milligan, D. E.; Jacox, M. E. Infrared Spectrum and Structure of Intermediates in the Reaction of OH with CO. *J. Chem. Phys.* **1971**, *54*, 927−942.
(8) Alagia, M.; Balucani, N.; Casavecchia, P.; Stranges, D.; Volpi, G. G. Crossed Beam Studies of Four-Atom Reactions: The Dynamics of OH + CO. *J. Chem. Phys.* **1993**, *98*, 8341−8344.
(9) Brouard, M.; Burak, I.; Hughes, D. W.; Kalogerakis, K. S.; Simons, J. P.; Stavros, V. Product State Resolved Stereodynamics: Rotational Polarization of OH($^2\Pi$, u', N', Ω, f) Scattered from the Reaction, H + CO_2 → OH + CO. *J. Chem. Phys.* **2000**, *113*, 3173−3180.
(10) Brouard, M.; Hughes, D. W.; Kalogerakis, K. S.; Simons, J. P. The Product Rovibrational and Spin−Orbit State Dependent Dynamics of the Complex Reaction H+CO_2→OH($^2\pi_i$;v,N,$\Omega_i f$)+CO: Memories of a Lifetime. *J. Chem. Phys.* **2000**, *112*, 4557−4571.
(11) Lester, M. I.; Pond, B. V.; Anderson, D. T.; Harding, L. B.; Wagner, A. F. Exploring the OH+CO Reaction Coordinate via Infrared Spectroscopy of the OH−CO Reactant Complex. *J. Chem. Phys.* **2000**, *113*, 9889−9892.
(12) Sears, T. J.; Radford, H. E.; Moore, M. A. B-Dipole Transitions in *trans*-HOCO Observed by Far Infrared Laser Magnetic Resonance. *J. Chem. Phys.* **1993**, *98*, 6624−6631.
(13) Sears, T. J.; Fawzy, W. M.; Johnson, P. M. Transient Diode Laser Absorption Spectroscopy of the ν_2 Fundamental of *trans*-HOCO and DOCO. *J. Chem. Phys.* **1992**, *97*, 3996−4007.
(14) Radford, H. E.; Moore, M. A.; Sears, T. J.; Grussdorf, J.; Nolte, J.; Temps, F. Far-Infrared Laser Magnetic Resonance of ^2X (A′) *trans*-DOCO. *J. Mol. Spectrosc.* **1994**, *165*, 137−149.
(15) Petty, J. T.; Moore, C. B. Transient Infrared Absorption Spectrum of the ν_1 Fundamental of *trans*-HOCO. *J. Mol. Spectrosc.* **1993**, *161*, 149−156.
(16) Petty, J. T.; Moore, C. B. Transient Infrared Absorption Spectrum of the ν_1 Fundamental of *trans*-DOCO. *J. Chem. Phys.* **1993**, *99*, 47−55.
(17) Oyama, T.; Funato, W.; Sumiyoshi, Y.; Endo, Y. Observation of the Pure Rotational Spectra of *trans*- and *cis*-HOCO. *J. Chem. Phys.* **2011**, *134*, 174303.
(18) Oyama, T.; Sumiyoshi, Y.; Endo, Y. Pure Rotational Spectra of the CO−*trans*-HOCO Complex. *J. Chem. Phys.* **2012**, *137*, 154307.
(19) Jacox, M. E. The Vibrational Spectrum of *trans*-HOCO Free Radical Trapped in Solid Argon. *J. Chem. Phys.* **1988**, *88*, 4598−4607.
(20) Forney, D.; Jacox, M. E.; Thompson, W. E. Infrared Spectra of *trans*-HOCO, $HCOOH^+$, and HCO_2^- Trapped in Solid Neon. *J. Chem. Phys.* **2003**, *119*, 10814−10823.
(21) Johnson, C. J.; Harding, M. E.; Poad, B. L. J.; Stanton, J. F.; Continetti, R. E. Electron Affinities, Well Depths, and Vibrational Spectroscopy of *cis*- and *trans*-HOCO. *J. Am. Chem. Soc.* **2012**, *133*, 19606.
(22) Fortenberry, R. C.; King, R. A.; Stanton, J. F.; Crawford, T. D. A Benchmark Study of the Vertical Electronic Spectra of the Linear Chain Radicals C_2H and C_4H. *J. Chem. Phys.* **2010**, *132*, 144303.
(23) Fortenberry, R. C.; Huang, X.; Francisco, J. S.; Crawford, T. D.; Lee, T. J. Vibrational Frequencies and Spectroscopic Constants from Quartic Force Fields for *cis*-HOCO: The Radical and the Anion. *J. Chem. Phys.* **2011**, *135*, 214303.
(24) Fortenberry, R. C.; Huang, X.; Francisco, J. S.; Crawford, T. D.; Lee, T. J. Quartic Force Field Predictions of the Fundamental Vibrational Frequencies and Spectroscopic Constants of the Cations $HOCO^+$ and $DOCO^+$. *J. Chem. Phys.* **2012**, *136*, 234309.
(25) Wang, Y. M.; Bowman, J. M. One-Dimensional Tunneling Calculations in the Imaginary-Frequency, Rectilinear Saddle-Point Normal Mode. *J. Chem. Phys.* **2008**, *129*, 121103.
(26) Johnson, C. J.; Continetti, R. E. Dissociative Photodetachment Studies of Cooled $HOCO^-$ Anions Revealing Dissociation Below the Barrier to H + CO_2. *J. Phys. Chem. Lett.* **2010**, *1*, 1895−1899.
(27) Johnson, C. J.; Poad, B. L. J.; Shen, B. B.; Continetti, R. E. Communication: New Insight into the Barrier Governing CO_2 Formation from OH+CO. *J. Chem. Phys.* **2011**, *134*, 171106.
(28) Ma, J.; Li, J.; Guo, H. Quantum Dynamics of the HO + CO → H + CO_2 Reaction on an Accurate Potential Energy Surface. *J. Phys. Chem. Lett.* **2012**, *3*, 2482−2486.

(29) Li, J.; Wang, Y. M.; Jiang, B.; Ma, J. Y.; Dawes, R.; Xie, D. Q.; Bowman, J. M.; Guo, H. Communication: A Chemically Accurate Global Potential Energy Surface for the HO+CO → H+CO_2 Reaction. *J. Chem. Phys.* **2012**, *136*, 041103.
(30) Nguyen, T. L.; Xue, B. C.; Weston, R. E.; Barker, J. R.; Stanton, J. F. Reaction of HO with CO: Tunneling Is Indeed Important. *J. Phys. Chem. Lett.* **2012**, *3*, 1549−1553.
(31) Davis, S.; Farnik, M.; Uy, D.; Nesbitt, D. J. Concentration Modulation Spectroscopy with a Pulsed Slit Supersonic Discharge Expansion Source. *Chem. Phys. Lett.* **2001**, *344*, 23−30.
(32) Davis, S.; Anderson, D. T.; Duxbury, G.; Nesbitt, D. J. Jet-Cooled Molecular Radicals in Slit Supersonic Discharges: Sub-Doppler Infrared Studies of Methyl Radical. *J. Chem. Phys.* **1997**, *107*, 5661−5675.
(33) Camy-Peyret, C.; Flaud, J. M.; Guelachvili, G.; Amiot, C. High Resolution Fourier Transform Spectrum of Water between 2930 and 4255 cm^{-1}. *Mol. Phys.* **1973**, *26*, 825−855.
(34) Hirota, E. *High-Resolution Spectroscopy of Transient Molecules*; Springer Series in Chemical Physics; Springer: Berlin, Germany, 1985; Vol. *40*.
(35) Sears, T. J.; Fawzy, W. M.; Johnson, P. M. Transient Diode-Laser Absorption-Spectroscopy of the ν_2 Fundamental of *trans*-HOCO and DOCO. *J. Chem. Phys.* **1992**, *97*, 3996−4007.
(36) Fortenberry, R. C.; Huang, X.; Francisco, J. S.; Crawford, T. D.; Lee, T. J. The *trans*-HOCO Radical: Quartic Force Fields, Vibrational Frequencies, and Spectroscopic Constants. *J. Chem. Phys.* **2011**, *135*, 134301.
(37) Wang, Y.; Carter, S.; Bowman, J. M. Variational Calculations of Vibrational Energies and IR Spectra of *trans*- and *cis*-HOCO Using New *Ab Initio* Potential Energy and Dipole Moment Surfaces. *J. Phys. Chem. A* **2012**, DOI: 10.1021/jp309911w.
(38) Oka, T.; Morino, Y. Calculation of Inertial Defect. 1. General Formulation. *J. Mol. Spectrosc.* **1961**, *6*, 472−482.
(39) Kroto, H. W. *Molecular Rotation Spectra*; Dover: New York, 1992.
(40) Duxbury, G. *Infrared Vibration−Rotation Spectroscopy: From Free Radicals to the Infrared Sky*; John Wiley & Sons Ltd: Chichester, England, 2000.
(41) Van Vleck, J. H. The Coupling of Angular Momentum Vectors in Molecules. *Rev. Mod. Phys.* **1951**, *23*, 213−227.
(42) Wick, G. C. On the Magnetic Field of a Rotating Molecule. *Phys. Rev.* **1948**, *73*, 51−57.
(43) Yumin, L.; Joseph, S. F. High Level *Ab Initio* Studies on the Excited States of HOCO Radical. *J. Chem. Phys.* **2000**, *113*, 7963−7970.
(44) Clements, T. G.; Continetti, R. E.; Francisco, J. S. Exploring the OH+CO → H+CO_2 Potential Surface via Dissociative Photodetachment of $HOCO^-$. *J. Chem. Phys.* **2002**, *117*, 6478−6488.
(45) Savee, J. D.; Mann, J. E.; Continetti, R. E. Dissociative Charge Exchange Dynamics of $HOCO^+$ and $DOCO^+$. *J. Phys. Chem. A* **2010**, *114*, 1485−1491.
(46) Huang, X.; Fortenberry, R. C.; Wang, Y.; Francisco, J. S.; Crawford, T. D.; Bowman, J. M.; Lee, T. J. Dipole Surface and Infrared Intensities for the *cis*- and *trans*-HOCO and DOCO Radicals. *J. Phys. Chem. A* **2012**, DOI: 10.1021/jp3102546.
(47) Scoles, G. *Atomic and Molecular Beam Methods*; Oxford University Press: New York, 1988; Vol. *1*.
(48) Lovejoy, C. M.; Nesbitt, D. J. Slit Pulsed Valve for Generation of Long-Path-Length Supersonic Expansions. *Rev. Sci. Instrum.* **1987**, *58*, 807−811.
(49) Lovejoy, C. M.; Nesbitt, D. J. Mode Specific Internal and Direct Rotational Predissociation in HeHF, HeDF, and HeHCl: van der Waals Complexes in the Weak Binding Limit. *J. Chem. Phys.* **1990**, *93*, 5387−5407.
(50) Lovejoy, C. M.; Schuder, M. D.; Nesbitt, D. J. Direct Ir Laser-Absorption Spectroscopy of Jet-Cooled CO_2HF Complexes — Analysis of the ν_1 HF Stretch and a Surprisingly Low-Frequency ν_6 Intermolecular CO_2 Bend. *J. Chem. Phys.* **1987**, *86*, 5337−5349.
(51) Nesbitt, D. J.; Lovejoy, C. M. Multiple Intermolecular Bend Vibrational-Excitation of a Hydrogen-Bond — An Extended Infrared Study of OCOHF. *J. Chem. Phys.* **1990**, *93*, 7716−7730.
(52) Ma, J.; Li, J.; Guo, H. Tunneling Facilitated Dissociation to H +CO_2 in $HOCO^-$ Photodetachment. *Phys. Rev. Lett.* **2012**, *109*, 063202.